Mott physics and the optical conductivity of electron-doped cuprates

A. J. Millis,[1,*] A. Zimmers,[2,3] R. P. S. M. Lobo,[2] N. Bontemps,[2] and C. C. Homes[4]
[1]*Department of Physics, Columbia University, 534 West 120th Street, New York, New York 10027, USA*
[2]*Laboratoire de Physique du Solide (UPR 5 CNRS) ESPCI, 10 rue Vauquelin 75231 Paris, France*
[3]*Center for Superconductivity Research, University of Maryland, College Park, Maryland 20742, USA*
[4]*Department of Physics, Brookhaven National Laboratory, Upton, New York 11973, USA*
(Received 5 November 2004; revised manuscript received 5 October 2005; published 29 December 2005)

The doping- and temperature-dependent conductivity of electron-doped cuprates is analyzed. The variation of kinetic energy with doping is shown to imply that the materials are approximately as strongly correlated as the hole-doped materials. The optical spectrum is fit to a quasiparticle scattering model; while the model fits the optical data well, factor of 3–4 inconsistencies with photoemission data are found, implying the presence of a large and doping-dependent Landau parameter.

DOI: 10.1103/PhysRevB.72.224517 PACS number(s): 74.72−h, 71.27+a, 74.25.Gz

I. INTRODUCTION

Despite 15 years of intensive study, many properties of the cuprate superconductors remain imperfectly understood. A crucial set of questions involves charge transport. Angle-resolved photoemission measurements[1] suggest the presence of reasonably well defined electronlike quasiparticle excitations characterized by a Fermi surface with position very close to that of band theory and a quasiparticle velocity only moderately renormalized from the band value. Optical measurements reveal a frequency-dependent conductivity[2,3] with a strong doping dependence and an integrated low-frequency absorption strength ("spectral weight") markedly smaller than that predicted by band theory.[4]

There is no generally accepted interpretation of the measured conductivity of high-T_c cuprates. Some authors argue that it may be understood in terms of quasiparticles scattered by a frequency- and temperature-dependent scattering rate;[2,5,6] others that it should be understood in more exotic terms.[7,8] Recently, the issue of the adequacy of a quasiparticle-only description has been reexamined:[9] for hole-doped materials at optimal doping, a model involving only quasiparticles with velocity and mean free path taken from angle-resolved photoemission experiments was shown to be inconsistent with the data.

A suppression of low-frequency optical oscillator strength is expected in materials, such as the high-T_c superconductors, which may be regarded as doped Mott insulators.[4] Our understanding of the physics of doped Mott insulators is far from complete. However, the development over the past 15 years of the "dynamical mean-field method" has provided an important theoretical step forward,[10] giving a practical (and in many cases apparently reliable) method for calculating properties of strongly correlated materials and leading to new insights into the one-electron (photoemission and specific-heat) properties of doped Mott insulators.[11] A crucial assumption in this method is that the electron self-energy depends much more strongly on energy than on momentum. This assumption may be theoretically justified in a limit of infinite spatial dimensionality. It implies that "vertex corrections" may be neglected, making the calculation of the optical conductivity straightforward once the electron self-energy has been determined. In other words, the key consequence of this theoretical approach is that the Mott correlations are expressed mainly through the electron self-energy, and in particular the suppression of low-frequency spectral weight occurring as the Mott phase is approached is caused by a divergence of the electron effective mass. An alternative class of theoretical approaches[12] involves ascribing the Mott spectral weight suppression to a "vertex correction" which diverges as the insulating phase is approached.

The experimental status of these predictions is unsettled. Good agreement between dynamical mean-field calculations and data has been found for electronically three-dimensional compounds such as V_2O_3 (Ref. 13). However, the applicability of the method to two-dimensional correlated materials is not clear. The discrepancies between the quasiparticle-only model and $Bi_2Sr_2CaCu_2O_{8+\delta}$ (BSCCO) optical data were interpreted by Ref. 9 as implying the presence of a relatively large vertex correction, but the evolution of the vertex correction with doping was not determined because only for optimally doped BSCCO was a consistent set of photoemission and optical data available. One implementation of the vertex correction idea, the slave-boson-gauge theory approximation,[12] has a reasonable qualitative correspondence with the measured conductivity, but has been shown to make predictions for the doping and temperature dependence of the superconducting penetration depth which disagree sharply with data.[14]

Recent experimental developments may offer a new perspective on the charge dynamics of high-temperature superconductors and therefore of low-dimensional Mott insulators. Improvements in sample preparation have led to a systematic set of measurements on *electron-doped* cuprate materials.[15–18] The electron-doped compounds, unlike the more extensively studied hole-doped compounds, display at $x \leqslant x_c \approx 0.15$ and at low enough temperature clear signatures of density wave behavior in the observed conductivity.[15–17,20] Recent theoretical works[21,22] have explained the difference in magnetic behavior between electron-doped and hole-doped compounds in terms of a model in which the electron-doped compounds exhibit "Mott" correlations which are weaker than in the hole-doped ones, and are doping-dependent.

In this paper, we undertake a systematic analysis of the conductivity measured on a series of films of electron-doped materials. The films were made at essentially the same time and under similar conditions, allowing an examination of the doping dependence of the conductivity. Measurements at lower temperatures and lower dopings reveal gaplike features which may be associated with antiferromagnetic order.[16,17] We consider data mainly at dopings and temperatures such that the density wave effects do not affect the analysis; a subsequent paper will report results of more detailed studies of density wave gap effects. We show that the magnitude and doping dependence of the kinetic energy implies that the electron-doped cuprates are approximately as strongly correlated as the hole-doped compounds. We further show that the canonical model of quasiparticles scattered by a (possibly large) self-energy is an inadequate description of the data.

The rest of this paper is organized as follows. In Sec. II we define the model and the quantities of interest. Section III presents the specific form of the self-energy used in our detailed analysis. Section IV presents discussion of the experiments we analyze. Section V gives an analysis of the qualitative features of the conductivity, in particular the kinetic energy and optical mass enhancement. Section VI presents an attempt to model the conductivity under the "no-vertex-corrections" approximation using the self-energy presented in Sec. III. Section VII outlines implications for the photoemission spectra and Sec. VIII is a conclusion.

II. MODEL

A. Overview

The conventional description of the motion of electrons in solids is in terms of electrons, propagating with a dispersion defined by a band-structure calculation and modified by a self-energy function expressing the effects of interactions not included in the band calculation. In this section, we present the band structure which seems likely to be relevant to the materials, and define the optical conductivity and related quantities including the "kinetic energy" which is a fundamental measure of the correlation strength of the materials.

B. Band structure

The band theory result for the conduction-band dispersion of high-T_c materials is well approximated by[23]

$$\varepsilon_p = -2t_1(\cos p_x + \cos p_y) + 4t_2 \cos p_x \cos p_y - 2t_3(\cos 2p_x + \cos 2p_y). \quad (1)$$

The parameters t_1, t_2, and t_3 have been obtained from band-theory calculations for a class of *hole-doped* compounds by a "down-folding" procedure;[23] canonical values are

$$t_1 = 0.38 \text{ eV}, \quad (2)$$

$$t_2 = 0.32t_1, \quad (3)$$

$$t_3 = 0.5t_2. \quad (4)$$

Studies have found significant variations of second- and third-neighbor hoppings between different cuprate material families.[24] However, the Fermi surface found in band-theory calculations performed directly on electron-doped materials[25] is almost identical to the Fermi surface following from Eqs. (1)–(4). Further evidence that these parameters provide a reasonable representation of the basic dispersion of the electron-doped materials comes from comparison to photoemission data.

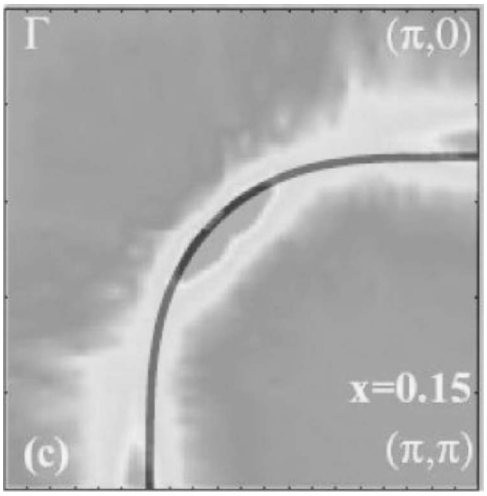

FIG. 1. Solid line: Fermi surface of electron doped cuprates at $x=0.17$ calculated from Eq. (1) using the standard band parameters given in the text and overlaid on a false-color representation of the near-chemical-potential photoemission intensity (Ref. 26) derived from angle-resolved photoemission measurements of an NCCO sample with nominal electron doping $x=0.15$. In this measurement, the Fermi surface is located in the light-shaded region.

For the energy dispersion implied by these parameters, at all relevant carrier concentrations the Fermi surface is hole-like [roughly circular, centered at the (π,π) point]. The Fermi surface implied by Eq. (1) for electron doping of $x=0.17$ is shown as the solid line in Fig. 1. It is overlaid on a false-color representation of the experimental near-Fermi-surface photoemission intensity.[26] In this measurement, the false-color conventions are such that the Fermi surface lies in the lighter-shaded region. (Other very recent measurements have found a slightly different shape;[27] the differences are too small to be relevant to the present paper.)

Note that although the correspondence between the calculated and measured Fermi surfaces is not perfect, it is reasonably good. Note also that the area enclosed by the calculated curve is equal to that enclosed by the measured one, suggesting that the actual doping of the region measured in the experiment is $x=0.17$, slightly higher than the nominal doping of $x=0.15$. The strong similarity between the calculation and the data appears to rule out the possibility of large differences in the underlying Fermiology between hole-doped and electron-doped materials, in particular contradicting the theoretical suggestion[28] that many-body physics effects could lead to a change in sign of t_2 between electron- and hole-doped materials. We believe that the agreement between the observed Fermi surface and the band-theory one justifies the use of the "canonical" tight-binding parameters in modeling the optical data.

In wide classes of "correlated electron" materials, standard band-theory calculations produce Fermi surfaces in rea-

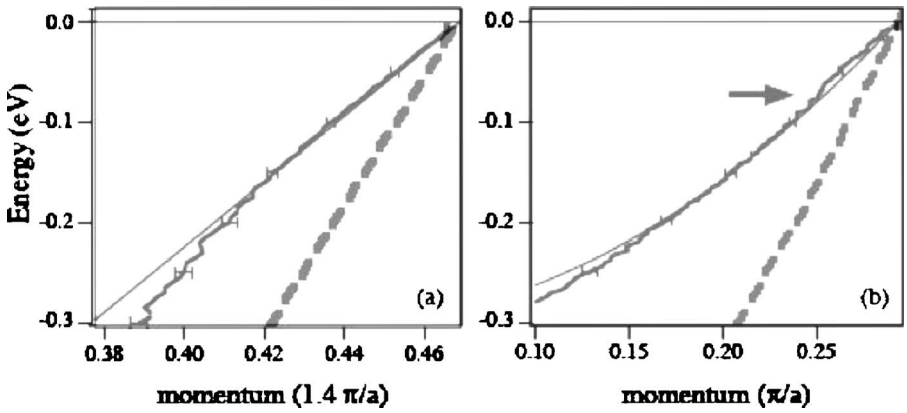

FIG. 2. Observed quasiparticle dispersions (heavy solid lines) from angle-resolved photemission measurements on $Nd_{1.85}Ce_{0.15}CuO_4$ (Ref. 26) compared to the tight-binding model prediction (dashed lines) and to the tight-binding model with hopping parameters reduced by a factor of 2 (light solid line). Panel (a): zone diagonal $[(0,0)\rightarrow(\pi,\pi)]$; Panel (b): zone face $[(\pi,0)\rightarrow(\pi,\pi)]$.

sonable agreement with experiment; however, electronic dispersions are often substantially renormalized. Figure 2 compares the dispersion obtained from angle-resolved photoemission measurements along two high-symmetry directions in the Brillouin zone to those obtained from the simple tight-binding parameters used above. One sees that in both symmetry directions the measured velocities are roughly half of the band velocities.

C. Optical conductivity

The optical conductivity $\sigma(\Omega)$ is the response function relating current to applied uniform, transverse electric field; it is given by

$$\sigma(\Omega)=\frac{e^2}{i\Omega}\int dt e^{-i\Omega t}\langle[\vec{j}(t),\vec{j}(0)]\rangle. \tag{5}$$

At frequencies below interband transitions, the current operator is $\vec{j}=(\partial\varepsilon_p/\partial\vec{p})c^{\dagger}_{p,\sigma}c_{p,\sigma}$. In particular, for current flow in the x direction we have (choosing units such that the in-plane lattice constant is unity)

$$\frac{\partial\varepsilon_p}{\partial p_x}=2t_1\sin p_x-4t_2\sin p_x\cos p_y+4t_3\sin 2p_x. \tag{6}$$

An important aspect of the conductivity is the spectral weight, or integrated area, which is most conveniently expressed as an energy via

$$K(\Omega)=\frac{\hbar c}{e^2}\int_0^{\Omega}\frac{2d\hbar\omega}{\pi}\sigma_1(\omega). \tag{7}$$

Here σ_1 is the real part of the observed conductivity and c is the c-axis lattice parameter. In this equation we have written ω as a frequency to conform to usual optics conventions. Henceforth in this paper we will write ω as an energy, suppressing the factor of $\hbar$ under the integrand. For convenience in converting between conventional and energy units, we note that $\hbar/e^2\approx 4k\Omega$.

Within band theory, the total kinetic energy associated with optical transitions within the conduction band is

$$K_{\rm band}=2\int\frac{d^2p}{(2\pi)^2}f(\varepsilon_p-\mu)\times(2t_1\cos p_x-4t_2\cos p_x\cos p_y+8t_3\cos 2p_x) \tag{8}$$

with f the Fermi function and μ the chemical potential. Numerical results for $K_{\rm band}$ are given in Table I; the relative doping dependence is seen to be weak in the whole doping range relevant to high-temperature superconductivity, and negligible for electron-doped materials.

Interactions are expected[4,29–31] to reduce K below its band-theory value; the amount of the reduction is a measure of the correlation strength.[4]

It is sometimes useful to express measured conductivities in terms of the optical mass m^* and scattering rate Γ defined via

$$-i\Omega\frac{m^*}{m_{\rm opt}}+\Gamma_{\rm opt}=\frac{K_{\rm band}}{\sigma_1(\Omega)+i\sigma_2(\Omega)}. \tag{9}$$

Note that the values obtained for $m^*/m_{\rm opt}$ and $\Gamma_{\rm opt}$ depend upon the normalization of the conductivity. We choose to normalize the conductivity to the band-theory kinetic energy, Eq. (8). Other choices would lead to different overall magnitudes for the optically defined mass and scattering rate, but would not change the relative frequency or temperature dependence. Typically in the literature the normalizing factor $K_{\rm band}$ is replaced by a value (smaller than $K_{\rm band}$) obtained by integrating the measured conductivity up to a frequency chosen according to some criterion. The normalization chosen here leads to a mass parameter which is precisely the mass enhancement relative to band theory.

TABLE I. Dependence of band kinetic energy on electron concentration n for hole ($n<1$) and electron ($n>1$) dopings.

n	0.8	0.9	1.0	1.1	1.2
$K_{\rm band}$ (eV)	0.38	0.41	0.42	0.43	0.42

A general expression for the conductivity is complicated.[9] If one makes the assumption that "vertex corrections" are negligible, then the conductivity becomes $\sigma = (e^2/\hbar c)(\Pi^{qp}/i\Omega)$ (in "imaginary time") with

$$\Pi^{qp}(\Omega) = T\sum_n \int \frac{d^2p}{(2\pi)^2} \times \mathbf{j}_x(p)\mathrm{Im}\, G(p,i\omega)\mathbf{j}_x(p)\mathrm{Im}\, G(p,i\omega + i\Omega) \tag{10}$$

and the Green function G given as usual by

$$G(p,i\omega) = \int_0^{1/T} d\tau e^{-i\omega\tau}\langle T_\tau d(\tau)d^\dagger(0)\rangle. \tag{11}$$

In particular, the dissipative part of the real-frequency conductivity is

$$\sigma_1^{qp}(\Omega) = \frac{e^2}{\hbar c}\int_{-\infty}^{\infty}\frac{d\omega}{\pi}\frac{[f(\omega) - f(\omega+\Omega)]}{\Omega} \times \int \frac{d^2p}{(2\pi)^2}\mathbf{j}_x(p)\mathrm{Im}\, G(p,\omega)\mathbf{j}_x(p)\mathrm{Im}\, G(p,\omega+\Omega). \tag{12}$$

Note that we have chosen units such that the in-plane momentum is dimensionless as is the product $j_x G$.

III. ELECTRON SELF-ENERGY

Doped Mott insulators generally, and cuprate materials in particular, appear[32] to be characterized by an electronic self-energy of unknown origin, which is not small and exhibits a significant temperature and frequency dependence. One widely used model self-energy is the "marginal Fermi liquid."[32] Another class of model self-energies, with many similar features, arises from "spin-fermion models" for materials near magnetic critical points.[33–35] The single-site dynamical mean-field method[10] leads to a qualitatively similar self-energy. The calculations reported below of the optical conductivity use a slightly different self-energy, of the form

$$\Sigma(\omega) = -i\gamma_{\mathrm{imp}} + i\Gamma(T)\left[1 - \lambda(T)\frac{\omega_c(\omega_c - i\omega)}{\omega_c^2 + \omega^2}\right] - Z\omega. \tag{13}$$

This form is chosen phenomenologically. It represents a self-energy with an imaginary part which is small at low frequency and large at high frequency, and without noticeable momentum dependence. This latter assumption is consistent with the photoemission data presented in the previous section.

Here γ_{imp} is a constant scattering rate assumed to come from impurities and the term $Z\omega$ expresses the effect of renormalizations arising from physics at energies above the highest frequencies considered in the analysis. The remaining "many-body" part of the self-energy is taken to be an inverted Lorentzian with frequency scale ω_c and overall strength Γ. The parameter $\lambda(T)$ controls the crossover from low to high frequency The key difference from the marginal Fermi liquid form is the presence of a scale, ω_c, which will be seen to be quite low. The real and (twice the) imaginary parts of the model self-energy are shown as heavy dashed lines in Fig. 3 for the parameters used in the calculation of the conductivity for the $x=0.17$ sample. Scattering rates extracted from analysis of the optical conductivity are also shown; these will be discussed below. The real part is displayed as a mass enhancement $m^*/m = 1 - \mathrm{Re}\,\Sigma(\omega)/\omega$.

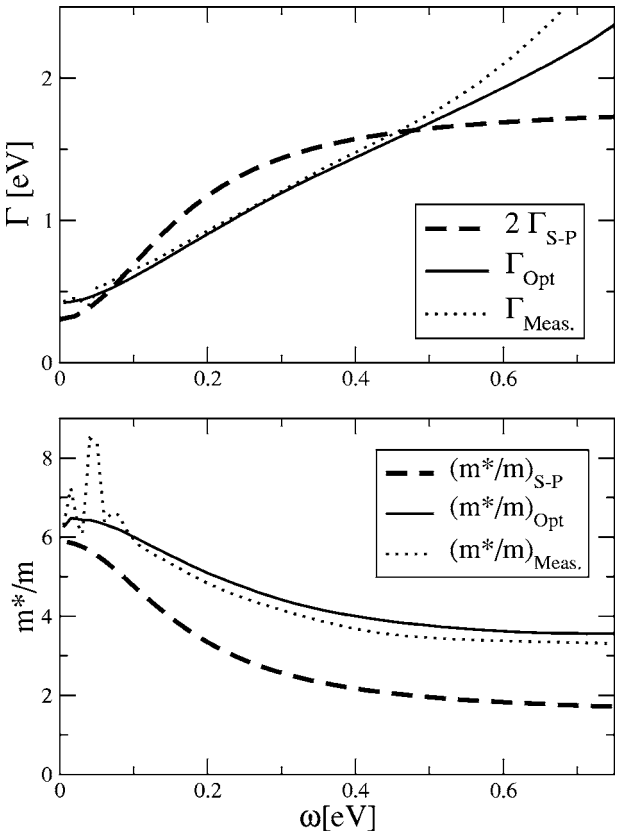

FIG. 3. Scattering rates (upper panel) and mass enhancements (lower panel) derived from room-temperature optical data for $x=0.17$ material, compared to results of fits and to corresponding single-particle rates. Light dotted lines: optically defined scattering rate Γ_{opt} and mass enhancement m^*/m_{opt} obtained from optical data using Eq. (9). Solid lines: Γ_{opt} and m^*/m_{opt} obtained by applying Eq. (9) to theoretical fit to optical conductivity. Heavy dashed lines: "single-particle" mass and (the negative of twice the) scattering rate obtained from model self-energy used in fits to $x=0.17$ room-temperature conductivity.

IV. EXPERIMENTAL ASPECTS

In this paper, we analyze in detail an extensive set of data obtained on thin films of $Pr_{2-x}Ce_xCuO_{4+\delta}$. To obtain an estimate of the uncertainties related to sample-to-sample differences, we compare the film data to room-temperature data from a PCCO single crystal[18,19] of nominal doping $x=0.15$ and transition temperature $T_c \approx 19$ K and to published measurements of a family of $Nd_{2-x}Ce_xCuO_{4+\delta}$ single crystals.[16] We compare one aspect of the electron-doped data (inte-

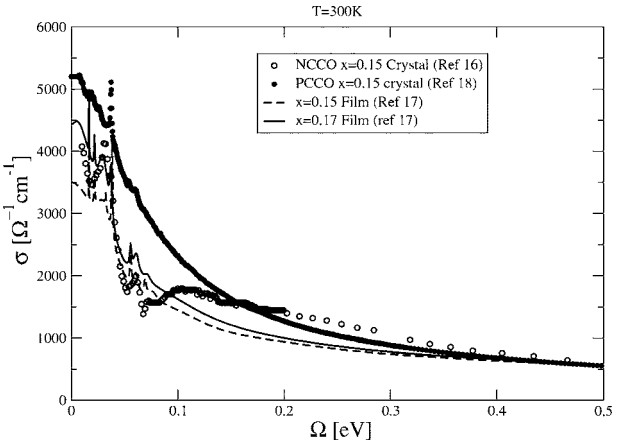

FIG. 4. Measured-room temperature conductivities of electron-doped cuprates at near-optimal doping.

grated optical weight) to a comprehensive set of data obtained by Lucarelli and co-workers[36,37] on the hole-doped analogue compound $La_{2-x}Sr_xCuO_{4-\delta}$ (LSCO).

Comparisons of different LSCO data sets reveal that for $x<0.2$ the data of Lucarelli and collaborators (Refs. 36 and 37) agree very well (within 5%) with the data obtained by Uchida *et al.* in 1991 (Ref. 3), for frequencies in the midinfrared regime ($\omega \gtrsim 0.1$ eV), suggesting that in LSCO compounds the materials issues are under control. The situation for electron-doped compounds is not yet as well converged.

The data and the specifics of the PCCO film growth and characterization have been presented elsewhere.[17,38] In brief, the films were epitaxially grown by pulsed-laser deposition on a $SrTiO_3$ substrate.[39] The Ce concentrations studied are (i) $x=0.11$ (thickness 2890 Å), (ii) $x=0.13$ (thickness 3070 Å), (iii) $x=0.15$ (thickness 3780 Å), and (iv) $x=0.17$ (thickness 3750 Å). Infrared-visible reflectivity spectra were measured for all samples in the 3 meV–3 eV spectral range with a Bruker IFS 66v Fourier transform spectrometer within an accuracy of 0.1% in relative value and ±0.5% in absolute value. For samples (iii) and (iv), which exhibit a large-weight and narrow "Drude peak" centered at $\omega=0$, the far-infrared (1.25–12.5 meV) frequency range was measured with a Bruker IFS 113v at Brookhaven National Laboratory using an *in situ* overcoating technique.[40] As discussed in detail elsewhere, the optical conductivity for the PCCO films was obtained from a standard thin-film fitting procedure.[17,38] Error bars in the conductivity were determined by detailed analytical calculations, numerical simulations,[38] and by varying the fitting parameters of the reflectivity and calculating the corresponding changes in the optical conductivity.[17] The $x=0.17$ film is opaque enough at low temperatures that substrate contributions are negligible, allowing the use of Kramers-Kronig analysis of the measured reflectivity. For this film, at low T (~20 K) errors were also determined by Kramers-Kronig transformations using different extrapolations.[44] All methods produced error bars in the optical conductivity of similar size (about 15% at low frequencies and 10% in the midinfrared).

The single crystal of $Pr_{2-x}Ce_xCuO_4$ was grown using a directional solidification flux growth technique in alumina

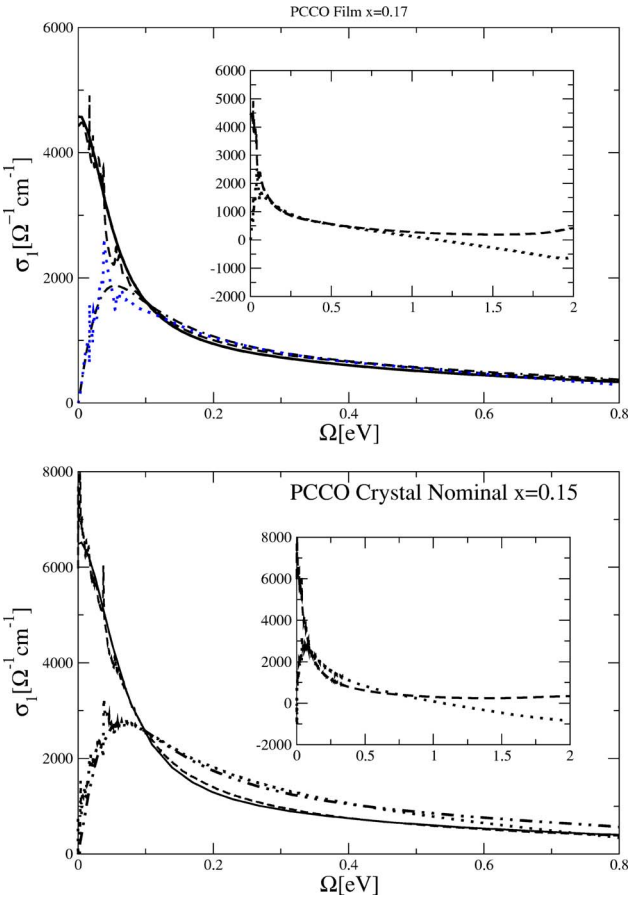

FIG. 5. (Color online) Main panels: real (dashed line) and imaginary (dotted line) parts of room-temperature measured conductivity of $x=0.17$ PCCO film (upper panel) and crystal (lower panel), compared to theoretical model (solid and dash-dot lines). Inset: measured conductivity over the wider frequency range 0–2 eV.

and high-purity magnesia crucibles.[41,42] The samples were then encapsulated into a pellet and powder setup similar to Ref. 43 and annealed in flowing argon at 900 °C for roughly a week to achieve optimal superconducting properties. Their superconducting transition was characterized using a Quantum Design SQUID magnetometer at 1 Oe in zero-field-cooling conditions. We note that although the nominal doping of this crystal was $x=0.15$, the relatively low transition temperature $T_c \approx 19$ K but relatively sharp transition suggests a rather higher doping, $x \gtrsim 0.17$. It has proven difficult to grow crystals with doping $x \gtrsim 0.18$. For purposes of further comparison, we assume the actual doping of the crystal to be $x=0.17$. The reflectance was measured at frequencies up to 4.3 eV (Ref. 40) and literature data were used to continue the reflectivity up to 30 eV. The systematic errors are of the order of 10%.

Relative uncertainties in the frequency and temperature dependence of one sample are relatively straightforward to quantify. Systematic errors, important in determining the absolute value of the conductivity of a given sample and therefore in the comparison of different samples, are more difficult to determine. We believe that the general level of uncertainty in the conductivity, arising from both relative and

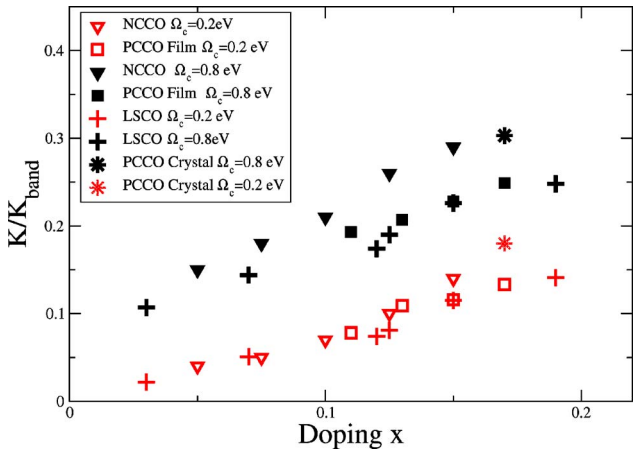

FIG. 6. (Color online) Kinetic energy for electron- and hole-doped cuprates, obtained by integrating measured room-temperature conductivities up to cutoff frequencies $\Omega_c=0.2$ eV and $\Omega_c=0.8$ eV and normalizing to the (doping-dependent; see Table I) band theory value, plotted against doping. The PCCO film data (squares) from Ref. 17 PCCO crystal data (stars) from Ref. 18, NCCO data (triangles) from Ref. 16, $La_{2-x}Sr_xCuO_4$ data (plus) from Refs. 36 and 37. Note that the doping for the PCCO crystal has been shifted from the nominal $x=0.15$ to the value $x=0.17$ inferred from the observed superconducting transition temperature

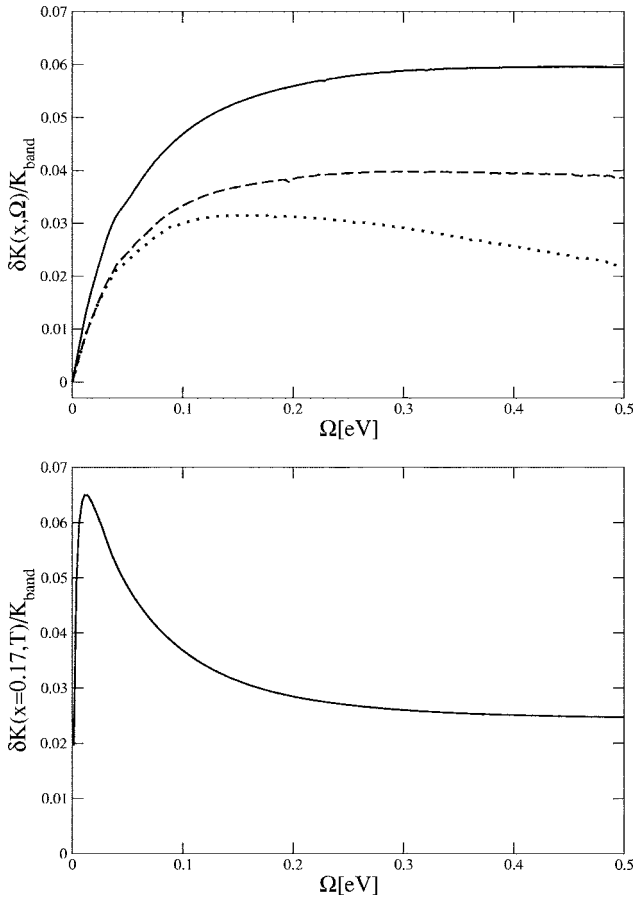

FIG. 7. Upper panel: Frequency dependence of difference in room-temperature kinetic energy between $x=0.11$ sample and $x=0.17$ (solid line), $x=0.15$ (dashed line), and $x=0.13$ (dotted line). Lower panel: Frequency dependence of difference of $T=25$ K and $T=300$ K kinetic energy of $x=0.17$ sample.

systematic errors in the measurement, is about 15%.

A potentially more significant source of uncertainty concerns variations among nominally similar samples arising either from possible intrinsic differences between films and crystals or between PCCO and NCCO, from difficulties in determining the actual doping level, and from possible inhomogeneity and randomness in the growth process. The difficulty is exacerbated in electron-doped materials by the need to expose the as-grown samples to a reducing atmosphere.

To demonstrate the uncertainties involved, we show in Fig. 4 the room-temperature conductivity obtained from several nominally similar samples: two PCCO films with nominal dopings $x=0.15$ and $x=0.17$, and two single crystals with nominal doping $x=0.15$: a PCCO crystal[18] and a NCCO crystal.[16] While the general magnitude and form of the conductivities are similar between different samples, significant differences exist. The NCCO crystal displays a clear midinfrared peak not seen in the other materials. In the PCCO films, such a peak is a signature of antiferromagnetism and is seen at room temperature only in PCCO films of much lower doping ($x\sim0.11$) (Ref. 17). The PCCO crystal exhibits a higher conductivity than the films or the NCCO material. As noted above, the actual doping of the PCCO crystal is probably higher than the nominal value, and it is conceivable that in the near-surface region probed by optics the actual doping is even higher than the mean doping in the material.

V. ANALYSIS OF DATA: KINETIC ENERGY AND MASS ENHANCEMENT

A. Overview

This section presents an analysis of important qualitative features of the observed conductivity, in particular the kinetic energy [Eq. (7)] and optical mass enhancement [Eq. (9)]. The analysis relies in an essential way on the assumption that in the frequency range of interest both the real and imaginary parts of the measured conductivity arise only from conduction-band carriers, with negligible effects of interband transitions. This assumption is clearly correct at very low frequencies, and clearly breaks down at sufficiently high frequencies. No sharply defined criterion has appeared in the literature for estimating a frequency below which the conductivity is dominated by the conduction band. This lack is a source of systematic error whose magnitude is at present unknown. The point of view taken here is as follows.

The insulating end-member Pr_2CuO_4 has a conductivity characterized by a gap at $\omega\approx1.5$ eV (Ref. 3). We believe that it is reasonable to regard this gap as the Mott-Hubbard (or charge-transfer) gap, and to attribute the absorption in the near-gap region (frequencies $\omega\sim1.5-2.5$ eV) mainly to conduction-band carriers excited above the Mott gap. Clearly, as the frequency is further increased, other processes (most likely transitions to "nonbonding" oxygen bands) become important. Modest doping (few percent) destroys the gap and redistributes optical-absorption strength from the immediate above-gap region to the range $0<\omega\sim1.5$ eV while not changing the interband transitions much.[3] We

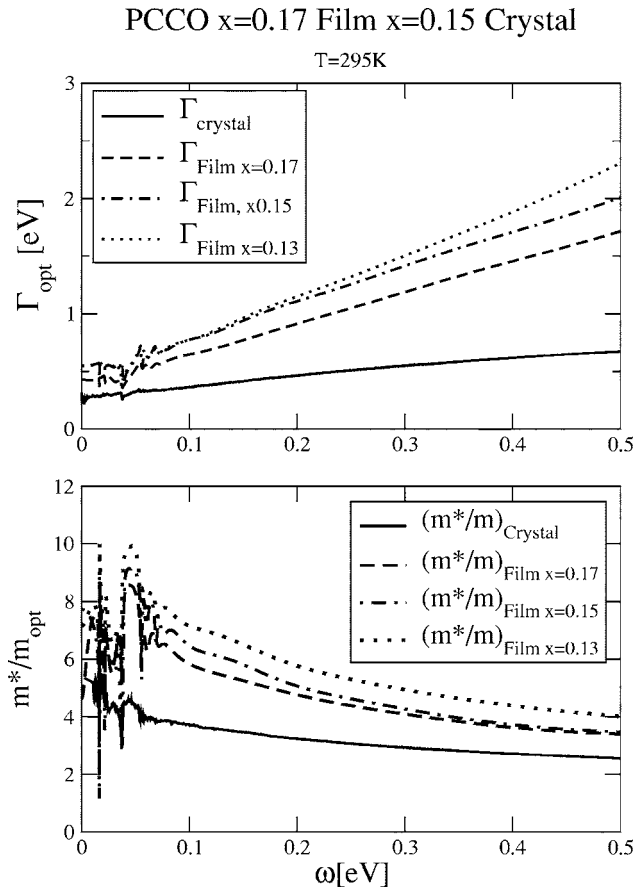

FIG. 8. Comparison of optical mass and scattering rate obtained from PCCO films and single crystal.

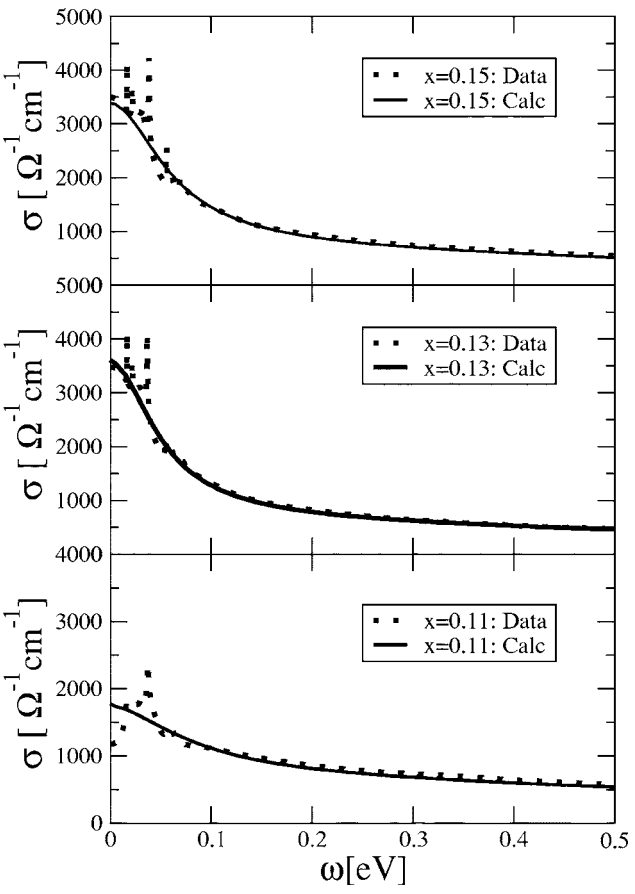

FIG. 9. Real part of the measured room-temperature conductivity (dashed lines) compared to theoretical model (solid lines) for $x=0.11$, 0.13, and 0.15.

therefore believe that at frequencies less than 1.5 eV, the observed absorption may be attributed to the conduction-band carriers of interest. However, an interband absorption at $\Omega > 1.5$ eV will produce a contribution to the reactive part of the conductivity at lower frequencies; thus only at frequencies substantially less than 1.5 eV will the total conductivity be dominated by the conduction-band carriers. Below, we present evidence suggesting that at the frequencies which are important for our analysis (frequencies less than about 0.5 eV), the interband contributions are negligible.

The insets of Fig. 5 display the measured conductivities of the $x=0.17$ film and crystal over a wide frequency range. The reactive part σ_2 displays a zero crossing at about $\Omega \approx 1-1.25$ eV; because the conduction-band contribution to σ_2 is non-negative, we believe that this arises from higher-frequency (interband) absorption features, including one whose onset is visible as the beginning of an upturn at the high end of the σ_1 frequency range. The assumption that both real and imaginary parts of σ are dominated by the conduction band clearly fails for frequencies higher than ~ 1.25 eV. To estimate more quantitatively the uncertainties involved, we observe that at frequencies below onset, an interband transition leads to a positive contribution $\delta\epsilon_{\mathrm{IB}}$ to the dielectric function ϵ. This corresponds to a negative imaginary contribution to the conductivity which, at frequencies well below the interband onset, is linear,

$$\delta\sigma_2(\omega) = -\frac{\omega}{4\pi}\delta\epsilon_{\mathrm{IB}}. \tag{14}$$

Fitting the observed linear variation of σ_2 (inset to Fig. 5) leads to $\delta\epsilon_{\mathrm{IB}} \approx 3.5$, in reasonable agreement with the common wisdom that in oxides the high-frequency dielectric constant is about $\epsilon_\infty \sim 5$. This estimate implies that at frequencies less than 0.75 eV, the interband contribution to σ_2 is small, and for frequencies below 0.5 eV it is of the order of 50 Ω^{-1} cm^{-1} or less, clearly completely negligible. Because our main results rely only on frequencies less than 0.5 eV, we believe that a neglect of the interband contribution is reasonable.

B. Kinetic energy

The kinetic energy defined in Eq. (7) is a fundamental measure of the strength of interactions. If the cuprates were well described by band theory, the low-frequency optical conductivity would consist of a narrow "Drude" peak concentrated at $\Omega=0$, with area leading to a kinetic energy $K(\Omega)$ which would rapidly approach the value $K_{\mathrm{band}}(x) \approx 0.4$ eV as Ω increases from 0.

Figure 6 shows the kinetic energy, obtained by integrating the room-temperature conductivity from zero to a cutoff frequency $\Omega_c=0.2$ eV and to $\Omega_c=0.8$ eV and normalizing to

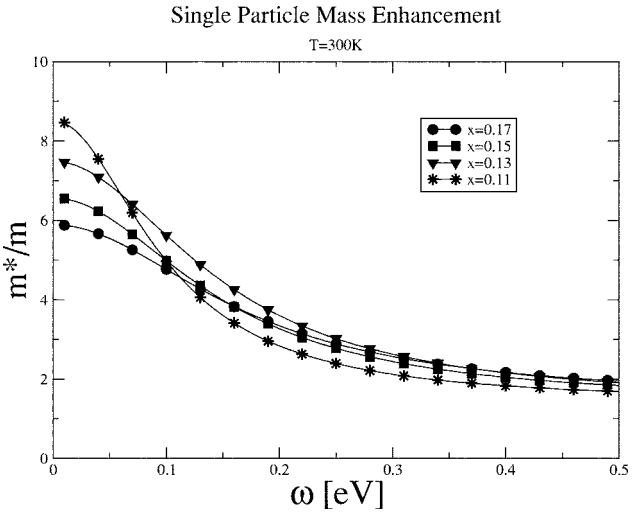

FIG. 10. Frequency-dependent single-particle mass enhancement $m^*/m = 1 - \mathrm{Re}\,\Sigma(\omega)/\omega$ inferred from self-energy only analysis of room-temperature conductivity.

the (doping-dependent) band value, plotted against doping. One sees that for all dopings, all materials, and all relevant frequencies, the kinetic energy is a very small fraction of the band value. A linear doping dependence is evident, with slope approximately independent of the cutoff frequency. The linear x dependence (with slope of the order of unity) and the small intercept are hallmarks of strong correlation or Mott physics.[4,29–31]

While most of the data on the figure pertain to the electron-doped cuprates, the figure shows as crosses the kinetic energy for the cognate hole-doped material $La_{2-x}Sr_xCuO_4$. The kinetic energy for this class of compounds was first studied in a pioneering paper by Uchida and co-workers.[3] More recent work[36,37] is (for the dopings we study here and in the midinfrared regime where both papers report data) consistent with the previous work of Ref. 3. The more recent data extend down to much lower frequencies, where (for LSCO, $x > 0.1$) a significant peak exists. For this reason the spectral weights reported in Refs. 36 and 37 and used in Fig. 6 are for $x > 0.1$, somewhat larger than those reported in Ref. 3.

One sees that the qualitative features of strong reduction in magnitude and strong doping dependence occur in both electron-doped and hole-doped materials. Further, within errors the measurements agree quantitatively, except that the "1/8 anomaly" visible[36] in the LSCO data is not evident in the electron-doped material.

The reasonable correspondences of the kinetic-energy magnitudes and doping dependencies suggest that the electron-doped materials are approximately as strongly correlated as the hole-doped ones. The approximately linear doping dependence of K suggests that the U value is not strongly doping-dependent within the electron-doped family of materials or indeed between electron- and hole-doped materials. Both of these observations are in apparent disagreement with recent theoretical studies of electron-doped compounds,[21,22] suggesting that despite the evident successes of these theories in accounting for the photoemission data, some issues remain in need of clarification.

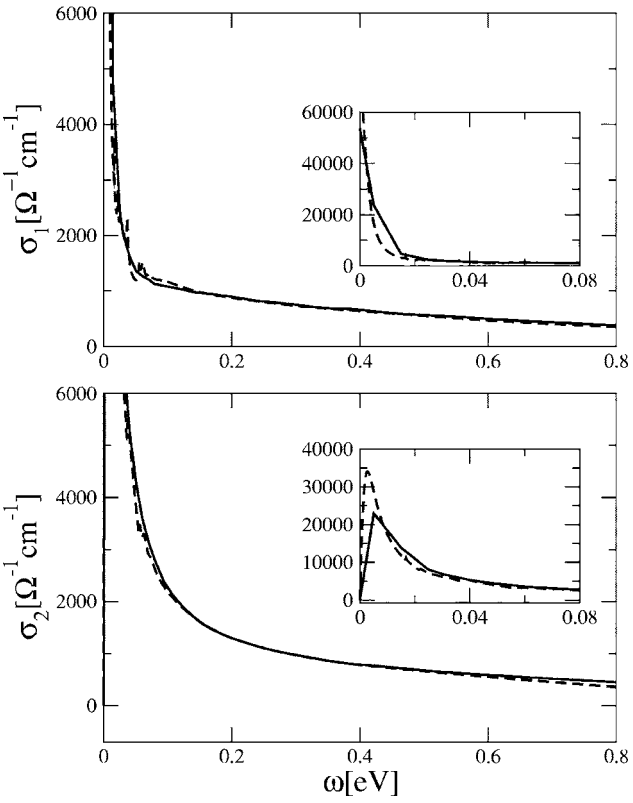

FIG. 11. Main panels: measured dissipative (upper) conductivity and reactive (lower) conductivities (dashed lines) compared to model calculation (solid lines) for $x = 0.17$ and $T = 25$ K. Inset: expanded view of the low-frequency regime.

As doping is increased, the optical conductivity increases, but the increase is not uniform in frequency. The upper panel of Fig. 7 shows the room-temperature kinetic energy difference $K(x,\Omega) - K(x = 0.11, \Omega)$ for $x = 0.13$, 0.15, and 0.17. A rapid rise at low frequency is evident, whereas the variation is much less at frequencies higher than about 0.15 eV; in other words, the doped carriers contribute most strongly to the low-frequency conductivity. The kinetic energy is also temperature-dependent, increasing as T is decreased. The lower panel of Fig. 7 shows the changes in the measured kinetic energy of the $x = 0.17$ sample as temperature is varied between room temperature and 25 K. As the temperature is varied, two effects may occur: a redistribution of spectral weight, arising because scattering rates and mass enhancements have temperature dependences, and a change in the total conduction-band spectral weight. Both effects are visible in the lower panel of Fig. 7: the sharp peak near zero frequency arises in part from a decrease in the scattering rate, which narrows the "Drude peak" leading to a pile-up of spectral weight at low frequency, while the saturation at higher frequencies shows that in addition to the rearrangement, there is a net temperature-dependent increase. The change in spectral weight as T is decreased from room temperature to 25 K in the $x = 0.17$ sample is seen to be of about the same magnitude as the increase in spectral weight as doping is increased from $x = 0.11$ to 0.17.

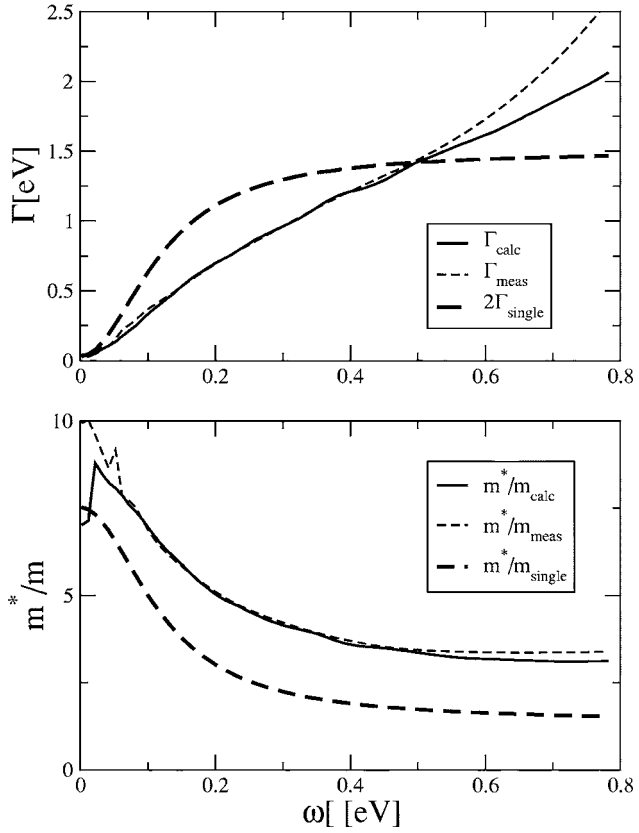

FIG. 12. The $T=25$ K scattering rate (upper panel) and mass enhancement (lower panel) derived from optical data (light dashed line), from theoretical fits to optical data for the $x=0.17$ sample (light solid line) compared to "single-particle" mass and scattering rate obtained from model self-energy (heavy dashed lines).

C. Mass and scattering rate

The dashed curves in Fig. 3 show the mass and scattering rate computed by applying Eq. (9) to the $x=0.17$ room-temperature data for frequencies up to about 6000 cm^{-1} ($\simeq 0.75$ eV). The light solid curves are obtained from a theoretical fit to σ discussed in detail in the next section. The upturn in the experimental optical scattering rate beginning at about 6000 cm^{-1} or 0.75 eV is caused mathematically by the decrease of σ_2 toward its 1.25 eV zero crossing. In physical terms, this is a signature that the data at $\omega \gtrsim 0.75$ eV are significantly affected by an interband transition, rendering an interpretation in terms of mass and scattering rate meaningless. The smooth behavior observed at lower frequencies, along with the analysis given above [see Eq. (13)], suggests that for frequencies below about 0.5 eV an interpretation in terms of a single band characterized by a mass and scattering rate is reasonable. The $\omega < 0.5$ eV data are consistent with an optical scattering rate which is reasonably linear in frequency, as in the hole-doped materials.[2,5]

Figure 8 shows the mass and scattering rates derived from the measured optical conductivity via Eq. (9) for the films studied here and for the crystal. The generic behavior is similar at all dopings and for film and crystal samples: the low-frequency optical mass enhancement (relative to band theory) is large, of order 4–8, even at room temperature, and is frequency-dependent. The optical scattering rate is approximately linear in frequency, and is also large. However, the differences between film and crystal data suggest precise intrinsic values of the mass and scattering rate are not yet well established experimentally. The trend with doping among films is consistent with the trend from film to crystal, perhaps suggesting that the crystal is more highly doped than the films (the reader should recall that all dopings are nominal, in particular because a reduction process is required to obtain superconductivity) but the quantitative differences suggest that further measurements and better sample characterization would be desirable.

The large mass is simply the restatement of the suppression of kinetic energy discussed above. In all cases, a high-frequency regime with relatively weak frequency dependence crosses over at a characteristic scale of roughly 0.25 eV to a lower-frequency regime with a stronger frequency dependence, and the high- and low-frequency masses differ by roughly a factor of 2. We believe that these data suggest that two processes are at work: an overall suppression of spectral weight (characterized by a frequency scale higher than the highest frequency we analyze) and an additional lower frequency ($\omega < 0.25$ eV) effect which enhances the mass by an additional factor of about 2.

VI. MODELING OF DATA

A. Overview

This section considers the modeling of the optical data within the no-vertex-corrections approximation. It begins with an analysis of the $x=0.17$ film, in which no signatures of density wave order are visible, and also presents by way of comparison an analysis of the crystal. The next subsection concerns the room-temperature behavior as a function of doping (where again no signatures of a density wave gap are evident except perhaps in the $x=0.11$ sample), and the final subsection deals with the effect of a density wave gap on the conductivity.

B. $x=0.17$

This section discusses the modeling of the $x=0.17$ optical data. A fundamental assumption, justified in detail above, is that the conductivity at scales less than 0.5 eV is described by a single band of carriers. The kinetic energy analysis of the previous section shows that the oscillator strength in the $\omega < 1$ eV conductivity is substantially less than is predicted by band theory. An analysis involving strong correlations is therefore needed. Here it will be assumed, consistent with the "single-site dynamical mean-field approximation"[10] and with many other works,[32–35] that the main effect of the correlations is to produce an electron self-energy which may be large and strongly frequency-dependent.

The solid and dash-dot lines in the upper panel of Fig. 5 show the results of theoretical calculations based on Eqs. (12) and (5), with $\Gamma=0.9$ eV, $\lambda=0.83$, $Z=0.5$, and $\omega_c=0.17$ eV. The agreement with data (dotted and dashed lines) is reasonable. The real and imaginary parts of the electronic self-energy are shown as heavy dashed lines in Fig. 3. The

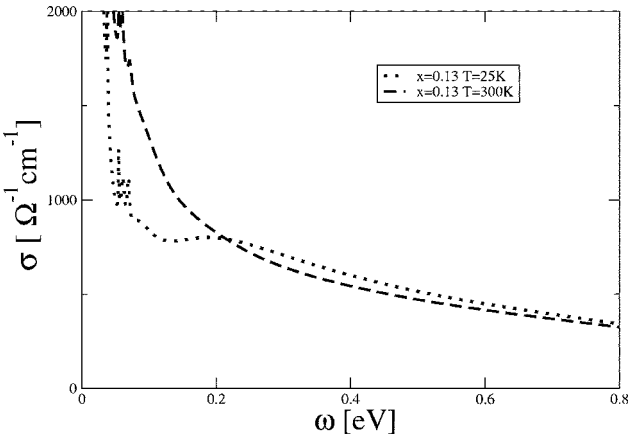

FIG. 13. Measured conductivity for $x=0.13$ sample at room temperature (dashed line) and low temperature (dotted line). A shift in spectral weight, characteristic of the opening of a density wave gap, is evident.

self-energy is characterized by a surprisingly low-frequency scale (0.17 eV) and by a very large magnitude. The high-frequency limit of the imaginary part of the self-energy is found to be frequency-independent, with a value ≈ 1 eV, comparable to the bandwidth. The low-frequency mass enhancement is correspondingly large (of order 6), and arises mostly from processes acting at the relatively low scale set by ω_c. The fits involve a function of several parameters, and it is therefore difficult to say precisely what are the uncertainties in the resulting values. However, Γ sets the rate at which the $\omega > 0.3$ eV conductivity drops with frequency, Z sets the magnitude of the conductivity in the high-frequency regime, λ sets the value at low ω, and ω_c determines the scale at which the behavior crosses over from low to high frequencies. Significant (more than 10%) changes in any one of these parameters leads to noticeable decreases in the quality of the fits.

It is evident from Fig. 3 that the optically defined mass and scattering rates are not faithful representations of the single-particle mass and scattering rates. In particular, the calculated optical scattering rate is much more nearly linear than is the imaginary part of the model single-particle self-energy, while the assumed single-particle mass drops off more quickly than the optically defined one.

To give some idea of the uncertainties involved, we show in the lower panel of Fig. 5 the same analysis for the PCCO crystal. One sees that the model provides an equally good parametrization of the crystal data, but of course the parameters are slightly different: $\Gamma=0.78$ eV, $\lambda=0.8$, $Z=0.35$, and $\omega_c=0.25$ eV. In particular, the broader and more "Drude"-like peak observed in the crystal leads to a higher fitted frequency scale, and the greater spectral weight evident at low frequency implies a weaker coupling and hence a lower mass.

C. Doping dependence

This subsection summarizes the results of fitting the room-temperature film conductivities with the quasiparticle-only model. Figure 9 shows the measured room-temperature conductivities and the best-fit calculated conductivities (solid lines) at the other available dopings $x=0.11$, 0.13, and 0.15. Figure 10 shows the single-particle mass enhancement inferred from these fits. The parameters are indicated in Table II.

Figure 10 shows that for $x=0.13$, 0.15, and 0.17, there is a negligible doping dependence of m^* at high frequencies while there is a characteristic, low-frequency scale below which the mass sharply increases, in a manner which depends on doping. This is a restatement, in the language of single-particle mass, of the observation made above that the effect of doping is to add spectral weight at low frequencies.

The $x=0.11$ sample is seen to deviate from the monotonic behavior. We will argue below and in a companion paper that this deviation is associated with the presence of antiferromagnetism even at room temperature.

For all dopings, the zero-frequency (Fermi surface) mass enhancements implied by the analysis are very large. As seen in Table II, this implies quasiparticle velocities substantially suppressed relative to band velocities.

D. Low-temperature analysis

Figure 11 shows data and model conductivities at low temperature (25 K). Again the agreement is reasonably good, although as can be seen from the inset the model underestimates the mass enhancement and overestimates the scattering rate at low frequencies. The "best-fit" parameters for the low-frequency data are $\Gamma=0.75$ eV, $\lambda=0.98, Z=0.4$, and $\omega_c=0.12$ eV. The decrease in Z reflects the increase in conduction-band kinetic energy; the increase in λ reflects the smaller value of the dc scattering rate; the decrease in Γ reflects the smaller value of the high-frequency optical scattering rate (more rapid decrease of σ_1) and the decrease in ω_c reflects the lower frequency and more rapid crossover of the data from high to low frequency. The actual value of the high-frequency conductivity has very little temperature dependence; thus, in this parametrization, changes in the parameters Z and Γ controlling the high-frequency conductivity must compensate each other. Figure 12 shows the single-particle and optically defined mass and scattering rate following from the fits to the low-temperature data. The qualitative behavior is very similar to that of the higher-temperature results.

Difficulties arise in applying this analysis to the low-T behavior of the lower x samples. The issue is most clearly revealed by examination of the data for $x=0.13$ sample. Comparisons of the dashed and dotted lines in Fig. 13 shows that as temperature is decreased the dissipative conductivity does not simply shift toward lower frequency, as does the conductivity of the $x=0.17$ material. Instead, an upward shift occurs in frequency, as expected if a density wave gap opens up. The conductivity of this material will be discussed in terms of antiferromagnetism in a companion paper.

VII. COMPARISON TO PHOTOEMISSION

The parameters obtained from the fits to the optical data make predictions for photoemission spectra. To facilitate

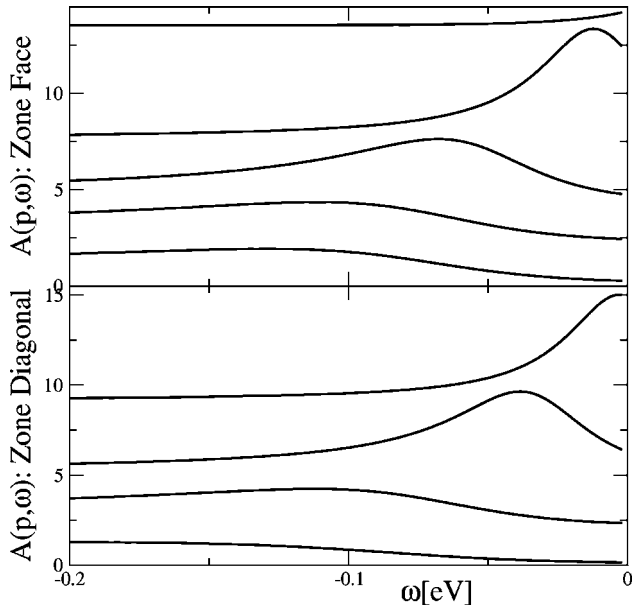

FIG. 14. Energy dispersion curves (electron spectral function as function of energy for fixed momentum) calculated for 300K best-fit optical parameters and shifted for clarity. Top panel: momenta along zone face $p=(\pi,(0,0.1,0.2,0.3,0.4)*\pi)$ highest curve, π, 0.4 π. Lower panel: zone diagonal, $p=0.2,0.3,0.4,0.45*(\pi,\pi)$ (highest curve, 0.45 π, 0.45 π).

comparison to experiment, we plot these as energy dispersion curves (EDC) which are the imaginary part of the electron Green function, plotted as a function of energy at fixed momentum. The two panels of Fig. 14 show EDC traces calculated using the self-energy which best fits the room temperature $x=0.17$ optics calculation.

The "no-vertex-corrections" modeling of the conductivity requires that the quasiparticle mass enhancement be very large in order to account for the suppression of spectral weight relative to band theory. The predicted Fermi velocity renormalizations are given in the last column of the table. These imply zone-diagonal Fermi velocities of order 0.5 eV Å, as may be seen directly from the dispersions of the peaks in Fig. 14. The velocities have been directly measured in photoemission experiments[26] and are found to be much larger, of order 1.5–2 eV Å, as may be seen in Fig. 2. This factor of 3–4 (or more) inconsistency shows that the self-energy-only model is not applicable to the electron-doped cuprates. In Fermi-liquid terms, a rather large vertex correction is important. Theories of the conductivity[6,34,35] which do not include a vertex correction seem unlikely to be directly applicable to the actual materials.

TABLE II. Self-energy parameters and associated velocity renormalization implied by self-energy-only analysis of room-temperature conductivity of films and (last row) PCCO crystal.

Doping	Γ (eV)	λ	ω_c (eV)	Z	v^*/v_{band}
0.11	0.95	0.75	0.1	0.41	0.12
0.13	1.1	0.83	0.15	0.41	0.13
0.15	0.98	0.79	0.15	0.41	0.15
0.17	0.9	0.83	0.17	0.5	0.17
CRY	0.78	0.80	0.25	0.35	0.25

VIII. CONCLUSION

We have presented a detailed analysis of the optical conductivity of a series of films of electron-doped cuprates, and have compared the results to other available data. Experiment presents a qualitatively consistent picture of the magnitude and general trends in the conductivity, although non-negligible variations occur between different materials (film vs crystal; NCCO vs PCCO). Further experimental and material effort to pin down the origin of the effect is needed.

We have shown, via an analysis of the kinetic energy, that the electron-doped materials are approximately as strongly correlated as the corresponding hole-doped systems. We have performed detailed modeling of the optical spectrum observed in films and a single crystal, using a self-energy which depends on frequency only. The essential assumption underlying this analysis is that at relevant frequencies the real and imaginary parts of the measured conductivity are dominated by the response of mobile carriers moving in the band structure inferred from band-theory calculations and scattered by some frequency- and temperature-dependent scattering mechanism. The optical response at low frequencies corresponds to a large (factor 4–10 depending on temperature and doping and material) mass enhancement relative to band theory; within the scattering-only model, this mass enhancement would imply a photoemission spectrum characterized by a velocity much (factor 3–4) lower than is actually observed. Uncertainties (for example related to the precise choice of band parameters and to the inevitable measurement uncertainties) are expected to be at most at the 10–20 % level, while sample-to sample differences lead to somewhat larger deviations. However, the discrepancy we found between the implied and measured Fermi velocity is much larger than the uncertainties.

We further note that the modeling was performed on the assumption that at frequencies less than $\approx$0.5 eV, the real and imaginary parts of the measured conductivity arise from scattered conduction-band carriers. For frequencies greater than about 0.75 eV, this assumption was shown to become untenable: a high-frequency interband transition produces a negative contribution to σ_2, leading to an unphysical upturn in the scattering rate (see Fig. 3 and Sec. IV C). Although we presented arguments that at frequencies less than 0.5 eV the absorptive part of the conductivity is due to conduction-band carriers, it remains possible that even at lower frequencies, interband transitions could appear. If this occurred, some of the optical oscillator strength presently assigned to the conduction band would be reassigned to an irrelevant transition; the optical masses would therefore be increased, worsening the discrepancy between optical and photoemission masses. We therefore suspect that our main finding, of a large discrepancy between the predictions of a self-energy-only theory and the photoemission and optical data, is robust.

Thus we conclude that the doping-dependent suppression of optical oscillator strength cannot be due solely to local

physics of the sort considered in the single-site dynamical mean-field theories of doped Mott insulators or in a variety of phenomenological models. As an aside, we find that the scattering rate inferred from an "extended Drude" analysis of the conductivity need not be a particularly faithful representation of the underlying single-particle scattering rate (see Fig. 3). Our conclusion is consistent with, and complementary to, an analysis recently presented by one of us[9] of the low-frequency optics and photoemission of optimally doped $Bi_2Sr_2CaCu_2O_{8+\delta}$. In this work, the very-low-frequency limit of the conductivity was compared to results of no-vertex-correction calculations performed using detailed photoemission momentum distribution curve (MDC) linewidths. Again a non-negligible vertex correction was found.

It is interesting to view this conclusion from a different perspective. The total conduction-band kinetic energy Eq. [7] may be alternatively expressed as

$$K = 2\sum_k \varepsilon_k n_k \tag{15}$$

with k-space occupancy n_k given by

$$n_k = \int \frac{d\omega}{\pi} \mathrm{Im}\, G(k,\omega) f(\omega) = \int \frac{d\omega}{\pi} \frac{\Sigma''(k,\omega)}{[\omega - \varepsilon_k - \Sigma'(k,\omega)]^2 + \Sigma''(k,\omega)^2} \tag{16}$$

with f the Fermi distribution function. In a noninteracting electron gas, n_k is just the usual Fermi distribution. The reduction of K due to interactions may be viewed in terms of a rearrangement of electron occupation more uniformly over the zone.[47] The strong observed reduction of K implies a strong redistribution of states; on the other hand, if interpreted within a frequency-dependent self-energy model, the relatively modest velocity renormalizations observed in photoemission experiments imply relatively modest self-energy effects and therefore relatively modest redistributions. A possible resolution is that a strong k dependence of Σ combines with a strong ω dependence to yield the observed relatively modest velocity renormalization. A strong k dependence of Σ implies that Landau renormalizations of the current are important.

Taken together, the available data present the following conundrum. Optical spectral weight is proportional to a carrier density times a charge squared divided by a carrier mass: $K \sim n_{\mathrm{eff}} e_{\mathrm{eff}}^2 / m_{\mathrm{eff}}$. Two conventional interpretations of a small spectral weight are a small number of carriers or a large carrier mass. The photoemission measurements reveal (at least for large dopings where density wave effects are absent) a large Fermi surface, consistent with band theory, and ruling out a simple small carrier number picture. Hall effect measurements[20] also indicate for optimally doped materials a carrier number reasonably consistent with the band-theory value. A large body of theoretical work[10,32–35] relates the form of the optical conductivity to a quasiparticle scattering rate and the spectral weight suppression to an enhanced quasiparticle mass. Our analysis shows that these theories require a mass enhancement larger by a doping-dependent factor of 2–5 than is directly observed in photoemission. One is therefore forced to look to a renormalization of the "effective charge." In Fermi-liquid language, this renormalization is expressed as a vertex correction or Landau parameter, so one must assume that the Mott correlations are expressed by a vertex correction which diverges as the doping decreases. The $U(1)$ slave boson formulation[12,45] of the Anderson RVB idea is one implementation of this idea; recent work of Benfatto *et al.*[46] is another. Unfortunately, these implementations of the vertex correction predict that the initial temperature dependence of the superfluid stiffness $d\rho_S/dT$ should vary approximately as the square of the doping; this prediction disagrees with data for a wide range of dopings.[14] Construction of a viable theory of the optical conductivity of this (and perhaps other) strongly correlated two-dimensional material remains an important open problem.

ACKNOWLEDGMENTS

We thank M. Ortolani and P. Calvani for very helpful discussions and for providing unpublished data; R. Greene for samples, assistance with characterization, and many helpful discussions; and P. Fournier and R. Greene for providing the PCCO single crystal. A.J.M acknowledges support from Grant No. NSF-DMR-0431350 and the CNRS. Work at Brookhaven was supported by the DOE under Contract No. DE-AC02-98CH10886.

*Corresponding author.

[1] A. Damascelli, Z. Hussain, and Z.-X. Shen, Rev. Mod. Phys. **75**, 473 (2003).
[2] J. Orenstein, G. A. Thomas, A. J. Millis, S. L. Cooper, D. H. Rapkine, T. Timusk, L. F. Scheemeyer, and J. V. Waszczak, Phys. Rev. B **42**, 6342 (1990).
[3] S. Uchida, T. Ido, H. Takagi, T. Arima, Y. Tokura, and S. Tajima, Phys. Rev. B **43**, 7942 (1991).
[4] A. J. Millis, *Optical Conductivity and Correlated Electron Physics*, in *Strong Interactions in Low Dimensions*, edited by D. Baeriswyl and L DeGiorgi (Springer Verlag, Berlin 2004).
[5] Z. Schlesinger, R. T. Collins, F. Holtzberg, C. Feild, S. H. Blanton, U. Welp, G. W. Crabtree, Y. Fang, and J. Z. Liu, Phys. Rev. Lett. **65**, 801 (1990).
[6] C. M. Varma and E. Abrahams, Phys. Rev. Lett. **86**, 4652 (2001).
[7] P. W. Anderson, Science **280**, 480 (2000).
[8] D. van der Marel *et al.*, Nature (London) **425**, 271 (2003).
[9] A. J. Millis and H. D. Drew, Phys. Rev. B **67**, 214517 (2003).
[10] A. Georges, G. Kotliar, W. Krauth, and M. J. Rozenberg, Rev. Mod. Phys. **68**, 13 (1996).
[11] M. Imada, A. Fujimori, and Y. Tokura, Rev. Mod. Phys. **70**, 1039 (1998).
[12] L. B. Ioffe and A. I. Larkin, Phys. Rev. B **39**, 8988 (1989).
[13] M. J. Rozenberg, G. Kotliar, H. Kajueter, G. A. Thomas, D. H.

Rapkine, J. M. Honig, and P. Metcalf, Phys. Rev. Lett. **75**, 105 (1995).
[14] L. B. Ioffe, and A. J. Millis, J. Phys. Chem. Solids **63**, 2259 (2002); see also A. J. Millis, S. M. Girvin, L. B. Ioffe, and A. I. Larkin, *ibid.* **59**, 1742 (1998).
[15] Y. Onose, Y. Taguchi, K. Ishizaka, and Y. Tokura, Phys. Rev. Lett. **87**, 217001 (2001).
[16] Y. Onose, Y. Taguchi, K. Ishizaka, and Y. Tokura, Phys. Rev. B **69**, 024504 (2004).
[17] A. Zimmers, J. M. Tomczak, R. P. S. M. Lobo, N. Bontemps, C. P. Hill, M. C. Barr, Y. Dagan, R. L. Greene, A. J. Millis, and C. C. Homes, Europhys. Lett. **70**, 225 (2005).
[18] C. C. Homes (unpublished).
[19] P. Fournier (private communication).
[20] Y. Dagan, M. M. Qazilbash, C. P. Hill, V. N. Kulkarni, and R. L. Greene, Phys. Rev. Lett. **92**, 167001 (2004).
[21] C. Kusko, R. S. Markiewicz, M. Lindroos, and A. Bansil, Phys. Rev. B **66**, 140513(R) (2002).
[22] B. Kyung, V. Hankevych, A.-M. Dare, and A.-M. S. Tremblay, Phys. Rev. Lett. **93**, 147004 (2004) and D. Senechal and A.-M. S. Tremblay, *ibid.* **92**, 126401 (2004).
[23] O. K. Andersen, A. I. Liechtenstein, O. Jepsen, and F. Paulsen, J. Phys. Chem. Solids **56**, 1573 (1995).
[24] E. Pavarini, I. Dasgupta, T. Saha-Dasgupta, O. Jepsen, and O. K. Andersen, Phys. Rev. Lett. **87**, 047003 (2001).
[25] S. Massida, N. Hamada, J. Yu, and A. Freeman, Physica C **157**, 571 (1989).
[26] N. P. Armitage *et al.*, Phys. Rev. Lett. **88**, 257001 (2002).
[27] T. Claesson, M. Mansson, C. Dallera, F. Venturini, C. De Nadai, N. B. Brookes, and O. Tjernberg, Phys. Rev. Lett. **93**, 136402 (2004).
[28] F. C. Zhang and T. M. Rice, Phys. Rev. B **37**, R3759 (1988).
[29] A. J. Millis and S. Coppersmith, Phys. Rev. B **42**, 10807 (1990).
[30] H. J. Schulz, Phys. Rev. Lett. **64**, 2831 (1990).
[31] C. A. Stafford and A. J. Millis, Phys. Rev. B **48**, 1409 (1993).
[32] C. M. Varma, E. Abrahams, S. Schmidt-Rink, and A. Ruckenstein, Phys. Rev. Lett. **63**, 1996 (1989).
[33] C. Jiang, E. Schachinger, J. P. Carbotte, D. Basov, and T. Timusk, Phys. Rev. B **54**, 1264 (1996).
[34] Branko P. Stojkovic and David Pines, Phys. Rev. B **55**, 8576 (1997).
[35] R. Haslinger, Andrey V. Chubukov, and Ar. Abanov, Phys. Rev. B **63**, 020503(R) (2000); see also Adv. Phys. **52**, 119 (2003).
[36] A. Lucarelli, S. Lupi, M. Ortolani, P. Calvani, P. Maselli, M. Capizzi, P. Giura, H. Eisaki, N. Kikugawa, T. Fujita, M. Fujita, and K. Yamada, Phys. Rev. Lett. **90**, 037002 (2003).
[37] M. Ortolani, P. Calvani, and S. Lupi, Phys. Rev. Lett. **94**, 067002 (2005), and private communication.
[38] A. F. Santander-Syro, R. P. S. M. Lobo, N. Bontemps, W. Lopera, D. Girata, Z. Konstantinovic, Z. Z. Li, and H. Raffy, Phys. Rev. B **70**, 134504 (2004).
[39] E. Maiser, P. Fournier, J.-L. Peng, F. M. Araujo-Moreira, T. Venkatesan, R. L. Greene, and G. Cjzek, Physica C **297**, 15 (1998).
[40] C. C. Homes, M. Reedyk, D. A. Crandles, and T. Timusk, Appl. Opt. **32**, 2972 (1993).
[41] J. L. Peng, Z. Y. Li, and R. L. Greene, Physica C **177**, 79 (1991).
[42] N. Kaneko, Y. Hidaka, S. Hosoya, K. Yamada, Y. Endoh, S. Takekawa, and K. Kitamura, J. Cryst. Growth **197**, 818 (1999).
[43] M. Brinkmann, T. Rex, H. Bach, and K. Westerholt, J. Cryst. Growth **163**, 369 (1996).
[44] A. Zimmers, R. P. S. M. Lobo, N. Bontemps, C. C. Homes, M. C. Barr, Y. Dagan, and R. L. Greene, Phys. Rev. B **70**, 132502 (2004).
[45] L. B. Ioffe and G. Kotliar, Phys. Rev. B **42**, 10348 (1990).
[46] L. Benfatto, S. Sharapov, N. Andrenacci, and H. Beck, Phys. Rev. B (to be published), e-print cond-mat/0407443.
[47] M. R. Norman, M. Randeria, B. Janko, and J. C. Campuzano, Phys. Rev. B **61**, 14742 (2000), and references therein.